

Distinct impacts of diverse forcing agents on Arctic sea ice since the mid-twentieth century

Yu-Chi Lee^{1*}, Wei Liu¹, Clara Deser², and Marika Holland²

¹Department of Earth and Planetary Sciences, University of California Riverside,
Riverside, CA, 92521, USA.

²Climate and Global Dynamics Laboratory, NSF-National Center for Atmospheric
Research, Boulder, CO, USA

Corresponding author: Yu-Chi Lee (yuchi.lee@email.ucr.edu)

Author Contributions

Y.-C.L. performed the analysis and wrote the original draft of the paper. W.L. conceived the study. Y.-C.L., W.L., C.D., and M.H. contributed to interpreting the results and made substantial improvements to the paper.

Abstract

Arctic sea ice has undergone non-monotonic changes since the middle of the last century. Here we investigate the cause of this behavior by isolating and quantifying the effects of anthropogenic aerosols, well-mixed greenhouse gases, and biomass burning on sea ice dynamics through climate model simulations. We find minimal changes in Arctic sea ice from 1956 to 1980, which primarily reflects a balance between the warming effect of greenhouse gases and the cooling effect of aerosols. This balance, however, is disrupted in subsequent decades. Both sea ice area and volume exhibit marked declines between 1981 and 2005, owing primarily to intensified warming by greenhouse gases and a shift in aerosol's role from mitigating to exacerbating sea ice loss. Our sea ice volume budget analysis demonstrates that sea ice changes since 1956 are mostly driven by thermodynamic processes: greenhouse gases significantly promote surface melt whereas aerosols and biomass burning diminish surface melt by reducing surface shortwave radiation in boreal summer. From 1956-1980 to 1981-2005, the transitional effects of aerosols are associated with increased bottom melting and decreased bottom ice formation, processes primarily driven by changes in the Atlantic meridional overturning circulation.

Main

Introduction

Arctic sea ice plays an essential role in Earth's climate system, significantly influencing albedo, heat exchange, and both atmospheric and oceanic circulation patterns^{1–6}. Since the late 1970s, satellite observations have documented a substantial decrease in the Arctic sea ice extent, with the most pronounced decline occurring in summer sea ice cover, particularly during September^{7–9}. This decline is attributed primarily to rising well-mixed greenhouse gas (GHG) emissions, which bring about intensified warming in the region^{10–13}.

Historical records, however, show a contrasting trend, with sea ice extent increasing between the 1950s to the 1970s^{14–16}. This earlier sea-ice increase stems from combined effects of increased anthropogenic aerosols (AAER) and natural climate variability, which temporarily counteracted GHG-warming through their cooling influences^{13,17,18}. Since the 1980s, reductions in AAER emissions especially in Europe and North America as a result of pollution control actions are thought to have contributed to Arctic surface warming and accelerating sea ice loss^{19–22}.

Unlike well-mixed GHGs, AAER exhibits pronounced temporal and spatial variability, which induces complex and regionally heterogeneous impacts on Arctic sea ice²³. Building on the historical influence of AAER on Arctic sea ice, understanding these effects is crucial, as further reductions in AAER in the coming decades are expected to have profound changes in Arctic sea ice²⁴. Biomass burning (BMB) emissions from forest fires, on the other hand, have also been suggested to influence the rate of Arctic sea ice loss over recent decades^{25–27}, adding another layer of complexity to the changes in Arctic climate system. Nonetheless, the precise physical processes through which the aforementioned climate forcings affect Arctic sea ice are not yet fully understood. In this context, investigating the historical response of Arctic sea ice to various external forcing agents, along with the underlying physical mechanisms, is essential for improving future projections, and this forms the central focus of our study.

Results

Distinct effects of different climate forcings on Arctic sea ice

We leverage large ensemble historical all-forcing and single-forcing simulations (Methods) with Community Earth System Model version 1 (CESM1) and climate models in Coupled Model Intercomparison Project phases 5 and 6 (CMIP5&6), most of which include multiple ensemble members (see Table S1 for more details), to investigate the effects of various forcing agents on Arctic sea ice. We examine Arctic sea ice area and volume during two key periods, 1956-1980 and 1981-2005, which are influenced by climate forcings in distinct ways (Fig. 1). Between 1956 and 1980, the CESM1 historical all-forcing ensemble shows minimal changes in total annual mean Arctic sea ice area and volume, consistent with observations (Fig. 1a and b), which also indicate an insignificant trend (see Tables S2 and S3). In terms of forcing agents, GHGs cause a significant decrease in sea ice, while AAER causes a significant increase. Our finding aligns with previous studies^{13,17,18}, which show that the opposing effects of GHGs and AAER during 1956-1980 counterbalance each other, leading to minimal changes in Arctic sea ice. BMB, meanwhile, also contributes to sea ice increases, albeit to a lesser extent than AAER does. Notably, the BMB-driven increase in sea ice area during this period is statistically insignificant, whereas the increase in sea ice volume is significant (see Tables S2 and S3). It merits attention that the multi-model mean of 4 CMIP5 and 9 CMIP6 models (Methods) supports these findings, with more than half of the models showing insignificant results. This further underscores the opposing effects of changing GHGs and AAER on Arctic sea ice (Fig. 1a and b).

The spatial pattern of annual mean linear trends of sea ice concentration from 1956 to 1980 in CESM1 reveals strong compensation between GHG-induced decreases and AAER-induced increases in the Beaufort, Chukchi, East Siberian, Greenland, and Kara-Barents Seas, as well as marginal seas in the North Pacific (Fig. 2b and c). Such cancelation explains the small changes in these areas when all climate forcings are included (Fig. 2a). The annual mean linear trends of sea ice thickness show a similar pattern of strongly compensating effects from GHG and AAER in the Beaufort, Chukchi, and East Siberian Seas (Fig. 2f and g). Notably, the annual mean linear trends of surface air temperature indicate corresponding warming from GHGs in regions experiencing larger declines in sea ice and cooling effects from AAER in areas with marked increases in sea ice (Fig. S1b and c). These temperature changes not only reflect the effects of the forcing agents but also likely contribute to

further sea ice changes via ice–albedo feedback, amplifying sea ice loss under GHG-induced warming^{12,28} and promoting ice retention under AAER-induced cooling.

In contrast, linear trends during the period 1981-2005 are strongly negative in the CESM1 all-forcing ensemble for both Arctic sea ice area and volume, which is consistent with the CMIP5&6 multi-model mean, as well as observations from the perspective of sea ice area (Fig. 1a and b; Table S2 and S3). Both GHGs and AAER contribute to this decline: GHGs induce a significant decrease, while AAER leads to smaller but still significant decreases. BMB contributes a relatively minor but significant increase for both Arctic sea ice area and volume. The CMIP5&6 multi-model mean shows similar effects from GHGs and AAER as in CESM1, but with weaker trends in sea ice area and volume, which is likely due to strong influence of internal climate variability¹¹.

Spatially, GHGs and AAER both lead to large reductions in sea ice concentration during 1981-2005 across the Arctic, including the Beaufort, Chukchi, East Siberian, Laptev, and Kara-Barents Seas, as well as marginal seas in the North Pacific (Fig. 3b and c). Some of these decreases are partially offset by increases due to BMB (Fig. 3d). Similarly, trends in sea ice thickness show significant declines near the East Siberian Sea due to the combined effects of GHGs and AAER, while BMB contributes to a modest increase around the Beaufort Sea (Fig. 3e, f, g, and h). It is noteworthy that the annual mean linear trends of surface air temperature during this period reflect not only the direct effects of the forcing agents but also the amplifying role of ice-albedo feedback as previous period. The significantly stronger warming in the Arctic due to GHGs (Fig. S1f) results from increased GHGs concentrations combined with a positive ice-albedo feedback that accelerates sea ice loss. On the other hand, a transition from cooling to warming effect by AAER (Fig. S1g) is likely due to reduced AAER emissions along with a warming influence that triggers a positive ice-albedo feedback. Meanwhile, general cooling over the Arctic associated with BMB (Fig. S1h) promotes sea ice formation.

Physical mechanisms

To investigate the physical processes by which climate forcings drive changes in Arctic sea ice, we examine the sea ice volume budget, taking into account both

dynamic and thermodynamic terms (Methods). The dynamic term accounts for sea ice volume changes induced by divergence/convergence and sea ice drift, while the thermodynamic term reflects changes due to ice formation and melting processes. Particularly, the thermodynamic term can be further decomposed into six components: ice formation over open ocean areas and at the base, conversion of snow to ice, ice melt at the top and base as well as lateral edges^{29,30}.

We first assess the integrated annual mean tendency of Arctic sea ice volume. From 1956 to 1980, the CESM1 all-forcing simulation displays a positive tendency, indicating a net increase of Arctic sea ice volume, which is due partly to the compensation between the strong increase from AAER and weaker decrease from GHGs (Fig. 4a). Further decomposition of the thermodynamic terms reveals that the effects of both changing GHGs and AAER primarily operate through alterations in the melting processes at the top of the ice, with GHGs contributing to increased melt and AAER leading to diminished melt (Fig. 4a). These processes predominantly occur during the boreal summer (Fig. S2). The increase in sea ice attributed to AAER is partially offset by reduced ice formation at ice base (Fig. 4a), which occurs in boreal fall and winter (Fig. S2e).

Seen from spatial patterns, AAER produces an overall positive sea ice volume tendency in the Arctic basin, with stronger increases in the Chukchi and East Siberian Seas (Fig. 4d). GHGs, on the other hand, create a negative sea ice volume tendency in the Arctic basin, with more pronounced declines in the Beaufort, Chukchi, and East Siberian Seas (Fig. 4c). Meanwhile, BMB generates much smaller sea ice volume tendencies with complex spatial patterns (Fig. 4e). As a result, the CESM1 all-forcing ensemble exhibits a net increase in sea ice volume in the Arctic basin, especially over the Chukchi Sea (Fig. 4b). Notably, these net tendencies reflect a compensation between thermodynamic and dynamic contributions. Specifically, the thermodynamic processes dominate the dynamic processes in the Arctic basin, whereas dynamic processes associated with ice convergence and divergence play a leading role around the Bering Strait and over the marginal seas in both the North Atlantic and Pacific (Fig. S4).

Between 1981 and 2005, CESM1 simulates a negative tendency in Arctic sea ice volume owing to both GHGs and AAER, with a slight offset from the moderate increase

by BMB (Fig. 5a-d). Both GHGs and AAER promote negative sea ice volume tendencies generally over the Arctic basin, with more conspicuous declines in the East Siberian Sea (Fig. 5c and d). On the contrary, BMB induces positive tendencies in the Beaufort and East Siberian Seas but negative tendencies in the Chukchi Sea (Fig. 5e). Notably, during this period, the interactions between thermodynamic and dynamic contributions are more complex. Specifically, in the Arctic basin, the thermodynamic contribution slightly outweighs the dynamic term for GHGs and BMB (Fig. S5b, d, f and h), whereas the dynamic contribution plays a more significant role for AAER (Fig. S5c and g). The pronounced dynamic effects for AAER are likely associated with the state-dependent feedbacks linked to thicker, more dynamically responsive ice. Consequently, in the historical all-forcing simulation, the dynamic contribution dominates over this region (Fig. S5a and e). However, this outcome may also reflect additional factors or nonlinear interactions among forcings that are not fully captured by the separate single-forcing simulations. Meanwhile, dynamic processes continue to dominate the net tendencies over the marginal seas in both the North Atlantic and Pacific (Fig. S5).

Our decomposition of the thermodynamic term indicates that, over 1981-2005, the GHG effect on sea ice volume is primarily through enhanced ice melting at the top and partly compensated by reduced ice melting at the base. AAER reduces ice melting at the top and base during summer (Fig. 5a and S3e). However, AAER's influence, which diminishes ice formation and promotes melt at the base during non-summer months, results in an overall negative impact on sea ice, occurring throughout most of the year. On the other hand, the BMB effect on sea ice volume manifests as reduced ice melting processes at the top during summer (Fig. 5a and S3f).

We further probe the net sea ice volume tendencies at both ice top and base, combining this analysis with surface heat fluxes and ocean heat and temperature budgets to identify the primary processes by which various forcing agents influence changes in Arctic sea ice. In the CESM1 historical all-forcing simulation, the net sea ice volume tendencies at the ice top during boreal summer (June-July-August, JJA) — when the surface heat flux is predominantly influenced by downward shortwave radiation — are negative from 1956 to 1980 over the Beaufort, Chukchi, East Siberian, and Kara Seas (Fig. 6a). In these regions, GHG-induced net sea ice volume

tendencies are weakly negative, accompanied by a moderate increase in surface downward shortwave radiation anomalies (Fig. 6b and f). Conversely, AAER-induced net sea ice volume tendencies are positive, along with a significant reduction in surface downward shortwave radiation anomalies (Fig. 6c and g). This reduction is most likely due to the direct effects of aerosols, which scatter incoming shortwave radiation and contribute to a cooling effect in the surface atmosphere^{29,31}.

In addition, these net tendencies are not solely determined by the direct radiative effects of the forcing agents. Changes in the physical state of the ice further modulate these responses through key feedback mechanisms^{10,32,33}. GHG-induced negative tendencies indicate thinning ice, which exposes darker surfaces and more open water and would enhance solar absorption via the ice-albedo feedback and further accelerate melting. In contrast, AAER tends to maintain thicker ice; this thicker ice acts as an insulator, reducing heat exchange with the underlying ocean and moderating further ice growth at the base. Together, these feedbacks amplify the net impacts of the forcing agents on changes of Arctic sea ice.

Between 1981 and 2005, CESM1 simulates similar annual mean net sea ice volume tendencies at the top during boreal summer across the Arctic to those in the previous period, with the exception of changes in the magnitude of shortwave radiation anomalies. Compared to 1956-1980, GHG-induced increases in surface downward surface radiation are amplified, whilst AAER-induced reductions are diminished (Fig. 7). These changes indicate that, under stronger GHG forcing, the positive ice-albedo feedback becomes even more effective, further accelerating melt. Conversely, the insulating effect of thicker ice associated with AAER is less pronounced in this later period, diminishing its capacity to offset melt. Moreover, the net sea ice volume tendencies by BMB are slightly positive over the Chukchi and East Siberian Seas, which correspond to a relatively smaller reduction in surface downward shortwave radiation (Fig. 7d and h).

The CESM1 all-forcing simulation, on the other hand, shows relatively weak positive annual mean net sea ice volume tendencies at ice base over the Arctic basin from 1956 to 1980, but much stronger negative tendencies in marginal ice zones such as the Bering, Barents, and Labrador Seas, as well as the area to the south of Greenland (Fig. 8a). These negative sea ice volume tendencies are mostly associated

with oceanic heat convergence induced by ocean circulation and warming tendencies (Fig. 8e) in both the Atlantic and Pacific sectors (Fig. 8a and e). In addition, these regional tendencies may also be influenced by dynamic ice processes, through ice convergence and divergence (Fig. S4a and e). Particularly, GHGs prompt negative sea ice volume tendencies over the central Arctic and positive tendencies in the marginal regions, accompanied by cooling tendencies in ocean temperatures on the Atlantic sector. Such oceanic cooling primarily results from a GHG-induced slowdown of the Atlantic meridional overturning circulation (AMOC) (Fig. S6). Different from GHGs, AAER engenders strong positive sea ice volume tendencies over the Beaufort and Kara-Barents Seas but negative tendencies in marginal ice zones of both the Pacific and Atlantic sectors (Fig. 8c). Such pattern corresponds to warming in ocean temperature in the subpolar Atlantic caused by AAER-induced AMOC strengthening^{34,35} (Fig. 8g and S6).

Between 1981 and 2005, GHGs further enhance the oceanic heat divergence and cooling in ocean temperature over the subpolar Atlantic (Fig. 9f) and thus promote the positive sea ice volume tendencies in the region. Meanwhile, AAER slightly amplifies the negative sea ice volume tendencies in the subpolar Atlantic (Fig. 9c) by increasing ocean heat convergence there (Fig. 9g). Note that while the strength of the AMOC shows a declining trend due to AAER reduction during this period, its average strength remains higher than the average of the previous period (Fig. S6). This finding is consistent with the results of Allen et al. (2024), who identify 1970 as a transition point for AAER's effects on the AMOC, with the AAER-induced strengthening persisting into the early decades of the twenty-first century. Compared to GHGs and AAER, BMB has the least impact on sea ice volume trends at ice base from 1956 to 2005 (Fig. 8d and 9d). Additionally, it is worth noting that the regional sea ice volume tendencies during this period may also be influenced by dynamic processes (Fig. S5).

Discussion

In this study, we investigate the distinct roles of different forcing agents in shaping Arctic sea ice dynamics using CESM1 all-forcing and single forcing large ensemble historical simulations. We discover that Arctic sea ice remains relatively stable from 1956 to 1980, owing primarily to a balance of opposing effects from GHGs and AAER.

This balance is upset in subsequent decades, resulting in a rapid decline in sea ice over 1981-2005. This shift can be attributed to the enhanced warming effects of GHGs and the reduction in AAER emissions from 1981 to 2005, which causes AAER's role to transition from mitigating to exacerbating sea ice loss. We further identify that all climate forcings significantly influence ice melting processes at the top during boreal summer. GHGs strongly promote sea ice melt at the top, whereas both AAER and BMB reduce it. The shifting role of AAER between 1981 and 2005 is attributed to its growing negative impacts on both the melting and formation processes at the ice base, which could be linked to the strengthened AMOC and persistent ocean warming in the subpolar North Atlantic. Additionally, the reduction in AAER emissions during this period increases incoming shortwave radiation over the Arctic basin, which would also directly enhancing ice melt at the surface. Our findings suggest that Arctic sea ice response to external forcings involves both fast adjustments through surface radiative fluxes and longer-term impacts via changes in ocean circulation.

Aside from AAER, BMB and well-mixed GHGs, other factors such natural climate variability^{13,18}, and anthropogenic changes in atmospheric ozone³⁶⁻³⁸ and ozone-depleting substances³⁶⁻³⁸ can also modulate Arctic sea ice, although their effects are generally weaker than those of AAER and GHGs^{17,18,36}. Moreover, the various climate forcings may have a complex and nonlinear interplay^{39,40}. As such, understanding the nuanced interactions between climate forcings, as well as their physical processes in governing sea ice dynamics, is of central importance. As the Arctic continues to change, ongoing monitoring and modeling efforts will be critical for accurately predicting future sea ice conditions.

Methods

Climate models and simulations

To isolate and quantify the responses of Arctic sea ice to various forcing agents, we employed CESM1 large ensemble all-forcing historical (HIST)⁴¹ and accompanying single forcing simulations⁴² (Table S1). The fully coupled CESM1 consists of Community Atmosphere Model version 5 (CAM5), Parallel Ocean Program version 2 (POP2), Community Land Model version 4 (CLM4), and Los Alamos Sea Ice Model (CICE) as described in detail in Hurrell et al. (2013). The all-forcing ensemble consist of 40 ensemble members, each of which is subject to the same historical forcing protocol but begin from slightly different initial conditions on 1 Jan 1920⁴¹. The single-forcing ensembles use the “all but” approach in which the forcing agent of interest is fixed at its 1920 level, while all other forcings vary over time⁴². There are three single-forcing ensembles: the fixed AAER forcing simulation (xAER) with 20 ensemble members, the fixed GHG forcing simulation (xGHG) with 20 ensemble members, and the fixed BMB forcing simulation (xBMB) with 15 ensemble members. Following the methodology outlined by Deser et al. (2020), we calculate the difference between the ensemble mean of the all-forcing and single forcing simulations to quantify the effects of AAER (HIST minus xAER), GHGs (HIST minus xGHG), and BMB (HIST minus xBMB). Note here these climate forcings may interact in a complex and nonlinear manner^{39,40}.

We also use available CMIP5&6 historical, GHG-only, and AAER-only simulations listed in Table S1. These CMIP5 and CMIP6 models adopt the “only” approach for the single forcing simulations, in which only the specific forcing (i.e., well-mixed GHGs or AAER) evolves over time during the historical period. Despite the differences in approaches between CMIP5&6 models and CESM1, we discovered that their results are fairly consistent.

Observations

We utilize the Arctic sea ice area products compiled by Walsh et al. (2019). The dataset integrates various historical observations, including ship reports, compilations from naval oceanographers, analyses conducted by national ice services, and satellite

passive microwave data, among other sources. The data are provided as monthly sea ice concentration on a $0.25^\circ \times 0.25^\circ$ longitude and latitude grid poleward of 30°N . Although the dataset extends back to 1850, our analysis focuses on the period from 1920 to 2005, aligning with the timeframe of the CESM1 climate model simulations employed in this research.

Sea ice volume budgets

We examine the sea ice volume budget that is based on the continuity equation:

$$\frac{dh}{dt} = \Gamma_h - \nabla(\vec{u}h) \quad (1)$$

where h denotes the mean ice thickness over a grid cell and \vec{u} denotes sea ice velocity. Γ_h is the thermodynamic source term, and $-\nabla(\vec{u}h)$ is the dynamic term, i.e., sea ice redistribution due to dynamic processes⁴⁵. Particularly, the thermodynamic source term Γ_h can be further decomposed into six terms: basal growth (congel), frazil growth (frazil), snow-ice conversion (snoice), basal melt (melbt), top melt (meltt) and lateral melt (meltl)²⁹. Integrated over the Northern Hemisphere, the dynamic term equals to zero, meaning that sea ice redistribution makes a zero net contribution to the total Arctic sea ice volume in the hemisphere.

The AMOC and associated oceanic processes

We define AMOC strength as the maximum of the annual mean meridional overturning stream-function below 500 m in the North Atlantic. Changes in the AMOC can affect ocean temperatures in the North Atlantic through advection and diffusion processes. This is represented by $tendency_{adv+diff}$, which is the vertically integrated ocean temperature advection and diffusion tendency per unit area.

Acknowledgements

This study has been supported by U.S. National Science Foundation (OCE-2123422, AGS-2053121, AGS-2237743, and AGS-2153486). The National Center for Atmospheric Research (NCAR) is sponsored by the National Science Foundation under Cooperative Agreement 1852977

References

1. Cohen, J. *et al.* Recent Arctic amplification and extreme mid-latitude weather. *Nat Geosci* **7**, 627–637 (2014).
2. Serreze, M. C. & Barry, R. G. *The Arctic Climate System*. (Cambridge University Press, 2014).
3. Curry, J. A., Schramm, J. L. & Ebert, E. E. Sea Ice-Albedo Climate Feedback Mechanism. *J Clim* **8**, 240–247 (1995).
4. Deser, C., Tomas, R. A. & Sun, L. The Role of Ocean–Atmosphere Coupling in the Zonal-Mean Atmospheric Response to Arctic Sea Ice Loss. *J Clim* **28**, 2168–2186 (2015).
5. Vihma, T. Effects of Arctic Sea Ice Decline on Weather and Climate: A Review. *Surv Geophys* **35**, 1175–1214 (2014).
6. Liu, W., Fedorov, A. & Sévellec, F. The Mechanisms of the Atlantic Meridional Overturning Circulation Slowdown Induced by Arctic Sea Ice Decline. *J Clim* **32**, 977–996 (2019).
7. Serreze, M. C., Holland, M. M. & Stroeve, J. Perspectives on the Arctic’s Shrinking Sea-Ice Cover. *Science (1979)* **315**, 1533–1536 (2007).
8. Stroeve, J., Holland, M. M., Meier, W., Scambos, T. & Serreze, M. Arctic sea ice decline: Faster than forecast. *Geophys Res Lett* **34**, (2007).
9. Serreze, M. C. & Stroeve, J. Arctic sea ice trends, variability and implications for seasonal ice forecasting. *Philosophical Transactions of the Royal Society A: Mathematical, Physical and Engineering Sciences* **373**, 20140159 (2015).
10. Holland, M. M., Bitz, C. M. & Tremblay, B. Future abrupt reductions in the summer Arctic sea ice. *Geophys Res Lett* **33**, (2006).
11. Stroeve, J. C. *et al.* Trends in Arctic sea ice extent from CMIP5, CMIP3 and observations. *Geophys Res Lett* **39**, (2012).
12. Notz, D. & Marotzke, J. Observations reveal external driver for Arctic sea-ice retreat. *Geophys Res Lett* **39**, (2012).
13. Mueller, B. L., Gillett, N. P., Monahan, A. H. & Zwiers, F. W. Attribution of Arctic Sea Ice Decline from 1953 to 2012 to Influences from Natural, Greenhouse Gas, and Anthropogenic Aerosol Forcing. *J Clim* **31**, 7771–7787 (2018).

14. Meier, W. N., Stroeve, J. & Fetterer, F. Whither Arctic sea ice? A clear signal of decline regionally, seasonally and extending beyond the satellite record. *Ann Glaciol* **46**, 428–434 (2007).
15. Mahoney, A. R., Barry, R. G., Smolyanitsky, V. & Fetterer, F. Observed sea ice extent in the Russian Arctic, 1933–2006. *J Geophys Res Oceans* **113**, (2008).
16. Semenov, V. A. & Latif, M. The early twentieth century warming and winter Arctic sea ice. *Cryosphere* vol. 6 1231–1237 Preprint at <https://doi.org/10.5194/tc-6-1231-2012> (2012).
17. Kong, N. & Liu, W. Unraveling the Arctic Sea Ice Change since the Middle of the Twentieth Century. *Geosciences (Switzerland)* **13**, (2023).
18. Gagné, M.-È., Fyfe, J. C., Gillett, N. P., Polyakov, I. V & Flato, G. M. Aerosol-driven increase in Arctic sea ice over the middle of the twentieth century. *Geophys Res Lett* **44**, 7338–7346 (2017).
19. Shindell, D. & Faluvegi, G. Climate response to regional radiative forcing during the twentieth century. *Nat Geosci* **2**, 294–300 (2009).
20. Acosta Navarro, J. C. *et al.* Amplification of Arctic warming by past air pollution reductions in Europe. *Nat Geosci* **9**, 277–281 (2016).
21. Ren, L. *et al.* Source attribution of Arctic black carbon and sulfate aerosols and associated Arctic surface warming during 1980–2018. *Atmos Chem Phys* **20**, 9067–9085 (2020).
22. Breider, T. J. *et al.* Multidecadal trends in aerosol radiative forcing over the Arctic: Contribution of changes in anthropogenic aerosol to Arctic warming since 1980. *Journal of Geophysical Research: Atmospheres* **122**, 3573–3594 (2017).
23. Wang, Y. *et al.* Elucidating the Role of Anthropogenic Aerosols in Arctic Sea Ice Variations. *J Clim* **31**, 99–114 (2018).
24. Gagné, M.-È., Gillett, N. P. & Fyfe, J. C. Impact of aerosol emission controls on future Arctic sea ice cover. *Geophys Res Lett* **42**, 8481–8488 (2015).
25. Schmeisser, L. *et al.* Seasonality of aerosol optical properties in the Arctic. *Atmos Chem Phys* **18**, 11599–11622 (2018).
26. Schmale, J., Zieger, P. & Ekman, A. M. L. Aerosols in current and future Arctic climate. *Nat Clim Chang* **11**, 95–105 (2021).
27. DeRepentigny, P. *et al.* Enhanced simulated early 21st century Arctic sea ice loss due to CMIP6 biomass burning emissions. *Sci Adv* **8**, eabo2405 (2025).

28. Screen, J. A. & Simmonds, I. The central role of diminishing sea ice in recent Arctic temperature amplification. *Nature* **464**, 1334–1337 (2010).
29. Holland, M. M., Bailey, D. A., Briegleb, B. P., Light, B. & Hunke, E. Improved Sea Ice Shortwave Radiation Physics in CCSM4: The Impact of Melt Ponds and Aerosols on Arctic Sea Ice*. *J Clim* **25**, 1413–1430 (2012).
30. Lee, Y.-C. & Liu, W. The Weakened Atlantic Meridional Overturning Circulation Diminishes Recent Arctic Sea Ice Loss. *Geophys Res Lett* **50**, e2023GL105929 (2023).
31. Li, J. *et al.* Scattering and absorbing aerosols in the climate system. *Nat Rev Earth Environ* **3**, 363–379 (2022).
32. Massonnet, F. *et al.* Arctic sea-ice change tied to its mean state through thermodynamic processes. *Nat Clim Chang* **8**, 599–603 (2018).
33. Bitz, C. M. & Roe, G. H. A Mechanism for the High Rate of Sea Ice Thinning in the Arctic Ocean. *J Clim* **17**, 3623–3632 (2004).
34. Chen, D., Sun, Q. & Fu, M. Aerosol in the subarctic region impacts on Atlantic meridional overturning circulation under global warming. *Clim Dyn* **62**, 9539–9548 (2024).
35. Allen, R. J., Vega, C., Yao, E. & Liu, W. Impact of industrial versus biomass burning aerosols on the Atlantic Meridional Overturning Circulation. *NPJ Clim Atmos Sci* **7**, 58 (2024).
36. Bushuk, M., Polvani, L. M. & England, M. R. Comparing the impacts of ozone-depleting substances and carbon dioxide on Arctic sea ice loss. *Environmental Research: Climate* **2**, 041001 (2023).
37. Sigmond, M. *et al.* Large Contribution of Ozone-Depleting Substances to Global and Arctic Warming in the Late 20th Century. *Geophys Res Lett* **50**, e2022GL100563 (2023).
38. Polvani, L. M., Previdi, M., England, M. R., Chiodo, G. & Smith, K. L. Substantial twentieth-century Arctic warming caused by ozone-depleting substances. *Nat Clim Chang* **10**, 130–133 (2020).
39. Simpson, I. R. *et al.* The CESM2 Single-Forcing Large Ensemble and Comparison to CESM1: Implications for Experimental Design. *J Clim* **36**, 5687–5711 (2023).
40. Deng, J., Dai, A. & Xu, H. Nonlinear Climate Responses to Increasing CO₂ and

- Anthropogenic Aerosols Simulated by CESM1. *J Clim* **33**, 281–301 (2020).
41. Kay, J. E. *et al.* The Community Earth System Model (CESM) Large Ensemble Project: A Community Resource for Studying Climate Change in the Presence of Internal Climate Variability. *Bull Am Meteorol Soc* **96**, 1333–1349 (2015).
 42. Deser, C. *et al.* Isolating the Evolving Contributions of Anthropogenic Aerosols and Greenhouse Gases: A New CESM1 Large Ensemble Community Resource. *J Clim* **33**, 7835–7858 (2020).
 43. Hurrell, J. W. *et al.* The Community Earth System Model: A Framework for Collaborative Research. *Bull Am Meteorol Soc* **94**, 1339–1360 (2013).
 44. Walsh, J. E., Chapman, W. L., Fetterer, F. & Stewart, J. S. Gridded Monthly Sea Ice Extent and Concentration, 1850 Onward. (G10010, Version 2). [Data Set]. Boulder, Colorado USA. National Snow and Ice Data Center (2019).
 45. Holland, M. M., Serreze, M. C. & Stroeve, J. The sea ice mass budget of the Arctic and its future change as simulated by coupled climate models. *Clim Dyn* **34**, 185–200 (2010).

Figures

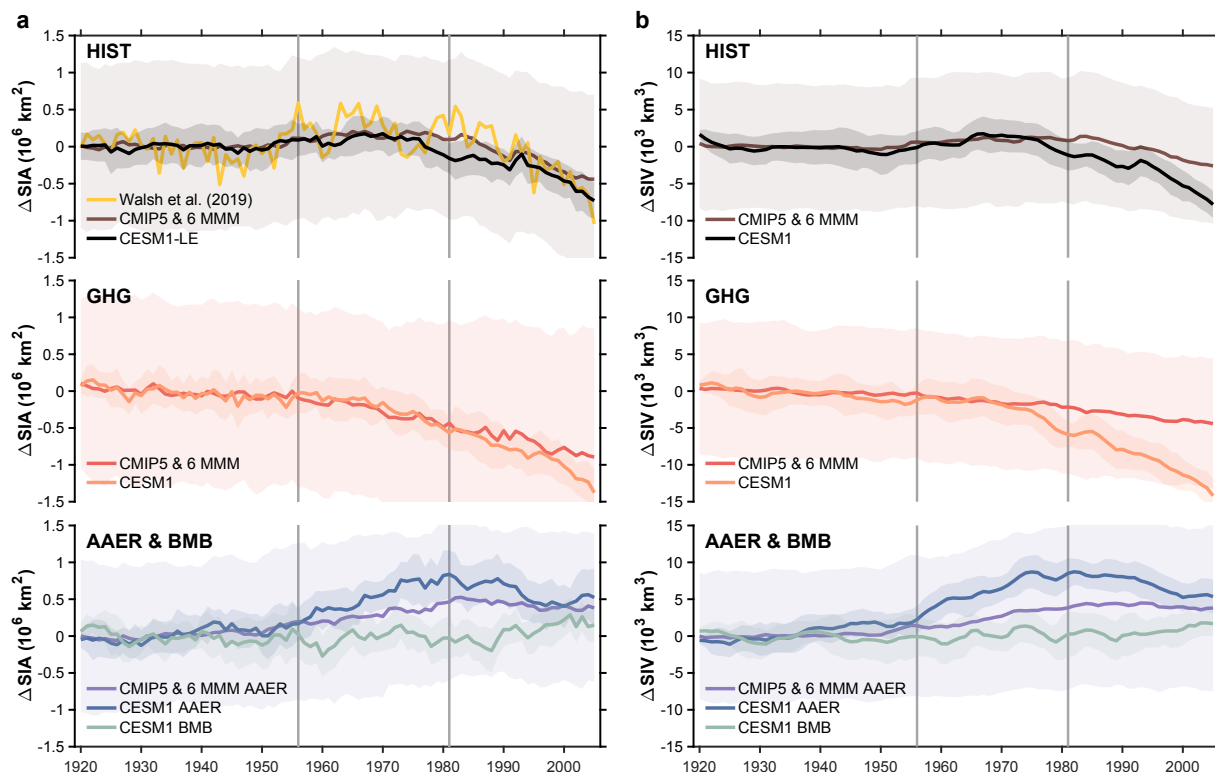


Fig. 1: Distinct effects of climate forcings on Arctic sea ice over the 20th century. (a) Annual mean sea ice area (SIA) and (b) sea ice volume (SIV) anomalies (relative to 1920-1945) during 1920-2005 for CESM1 historical ensemble mean (HIST: black line), CMIP5 & CMIP6 multi-model mean (CMIP5 & 6 MMM) (brown), and observations (yellow), and contributions from well-mixed greenhouse gases (GHGs: orange for CESM1 ensemble mean, red for CMIP5 & CMIP6 MMM), anthropogenic aerosols (AAER: blue for CESM1 ensemble mean, purple for CMIP5 & CMIP6 MMM), and biomass burning (BMB: green for CESM1 ensemble mean). Light-colored shadings represent one standard deviation across ensemble members for each simulation. CMIP5 & CMIP6 MMM is derived from four CMIP5 and nine CMIP6 models.

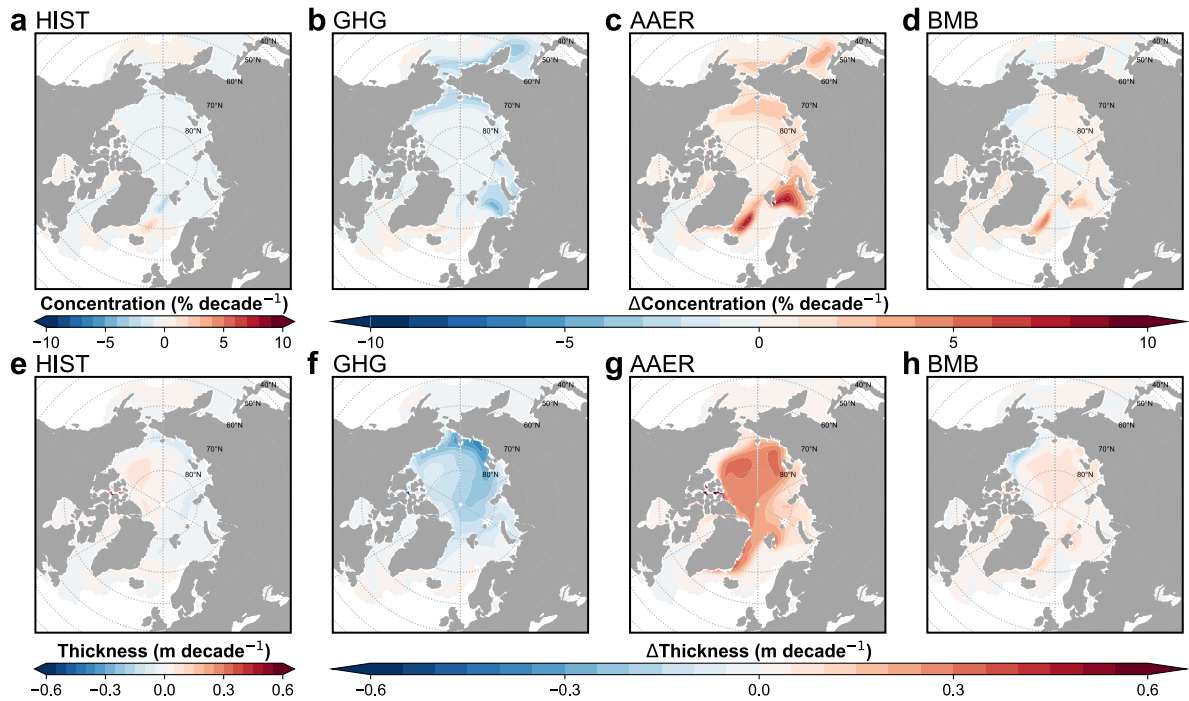


Fig 2: Trends in Arctic sea ice concentration and thickness (1956-1980) under different forcing agents in CESM1. Linear trends from 1956 to 1980 of annual and ensemble mean **(a-d)** sea ice concentration (shading in $\% \text{ decade}^{-1}$) and **(e-h)** sea ice thickness (shading in m decade^{-1}) in the Arctic. (a,e) for historical climate forcings (HIST), (b,f) for well-mixed greenhouse gases (GHG), (c,g) for anthropogenic aerosols (AAER), and (d,h) for biomass burning (BMB).

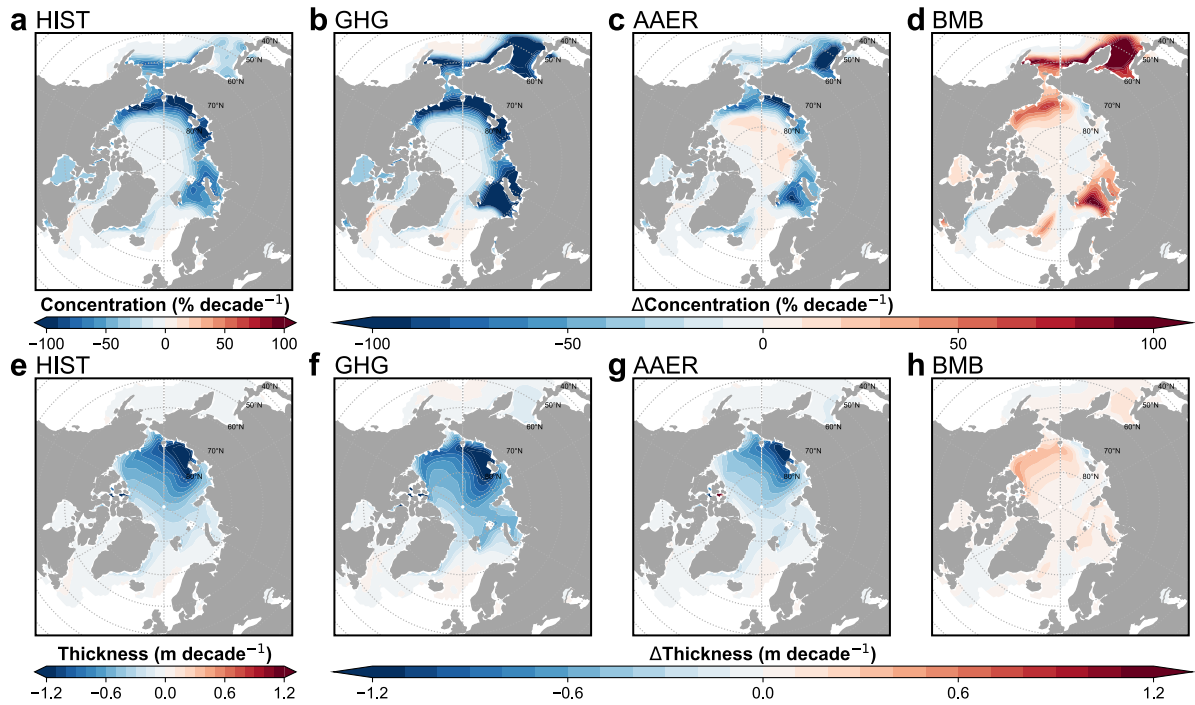


Fig 3: Trends in Arctic sea ice concentration and thickness (1981-2005) under different forcing agents in CESM1. Linear trends from 1981 to 2005 of annual and ensemble mean (a-d) sea ice concentration (shading in $\% \text{ decade}^{-1}$) and (e-h) sea ice thickness (shading in m decade^{-1}) in the Arctic. (a,e) for historical climate forcings (HIST), (b,f) for well-mixed greenhouse gases (GHG), (c,g) for anthropogenic aerosols (AAER), and (d,h) for biomass burning (BMB).

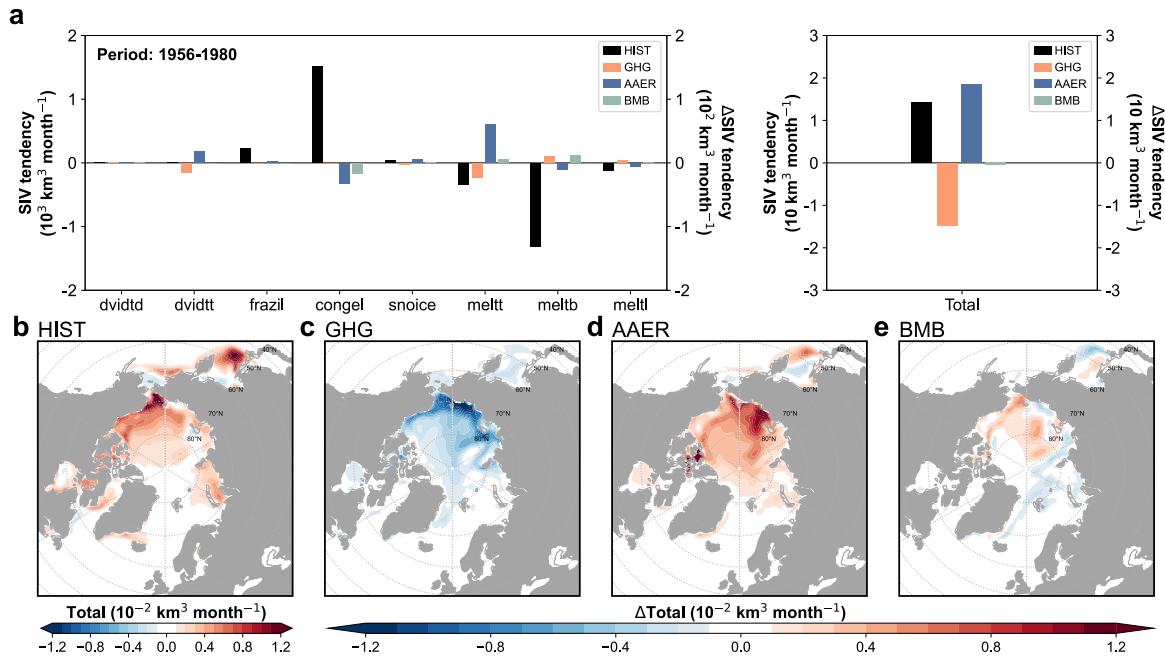


Fig 4: Arctic sea ice volume budgets and spatial patterns (1956-1980) under different forcing agents in CESM1. (a) Integrated annual and ensemble mean Arctic sea ice sea ice volume tendency terms for the period 1956-1980, with the left y-axis representing historical values (HIST: black bars) and the right y-axis showing the relative contributions from well-mixed greenhouse gases (GHG: orange bars), anthropogenic aerosols (AAER: blue bars), and biomass burning (BMB: green bars). Note that values on the right y-axis are scaled down by a factor of 10 compared to the left y-axis for left panel in (a). **(b-e)** Annual and ensemble mean net sea ice volume tendencies (shading in $10^{-2} \text{ km}^3 \text{ month}^{-1}$) caused by (b) historical climate forcings (HIST), (c) well-mixed greenhouse gases (GHG), (d) anthropogenic aerosols (AAER), and (e) biomass burning (BMB).

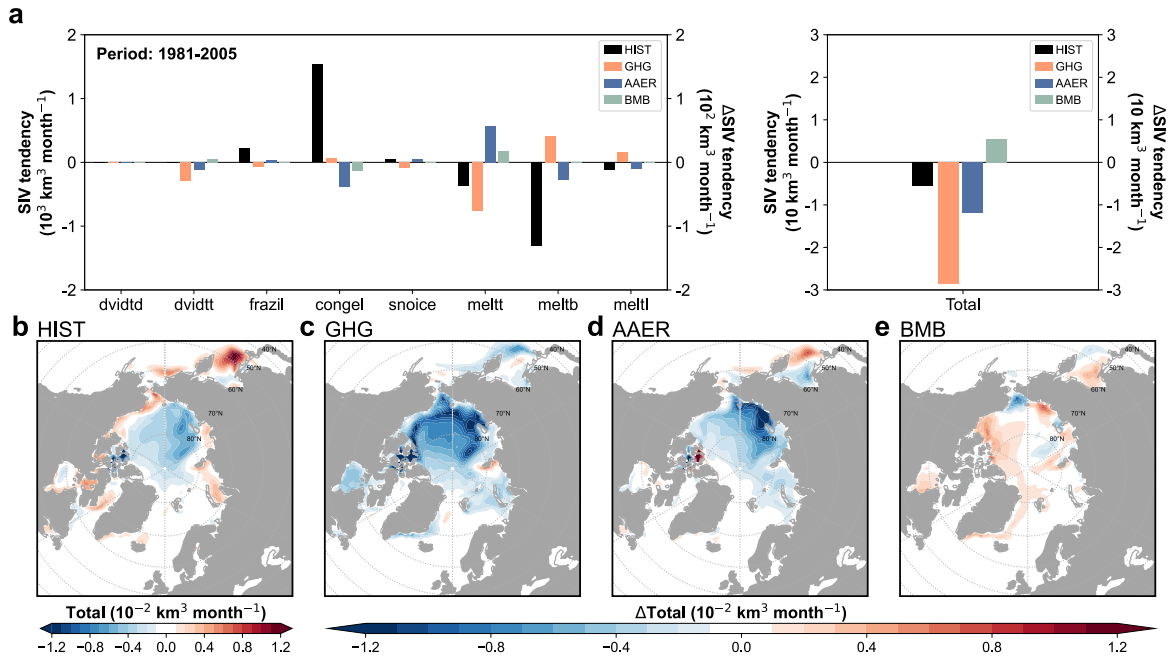


Fig 5: Arctic sea ice volume budgets and spatial patterns (1981-2005) under different forcing agents in CESM1. (a) Integrated annual and ensemble mean Arctic sea ice sea ice volume tendency terms for the period 1981-2005, with the left y-axis representing historical values (HIST: black bars) and the right y-axis showing the relative contributions from well-mixed greenhouse gases (GHG: orange bars), anthropogenic aerosols (AAER: blue bars), and biomass burning (BMB: green bars). Note that values on the right y-axis are scaled down by a factor of 10 compared to the left y-axis for the left panel in (a). **(b-e)** Annual and ensemble mean net sea ice volume tendencies (shading in $10^{-2} \text{ km}^3 \text{ month}^{-1}$) caused by (b) historical climate forcings (HIST), (c) well-mixed greenhouse gases (GHG), (d) anthropogenic aerosols (AAER), and (e) biomass burning (BMB).

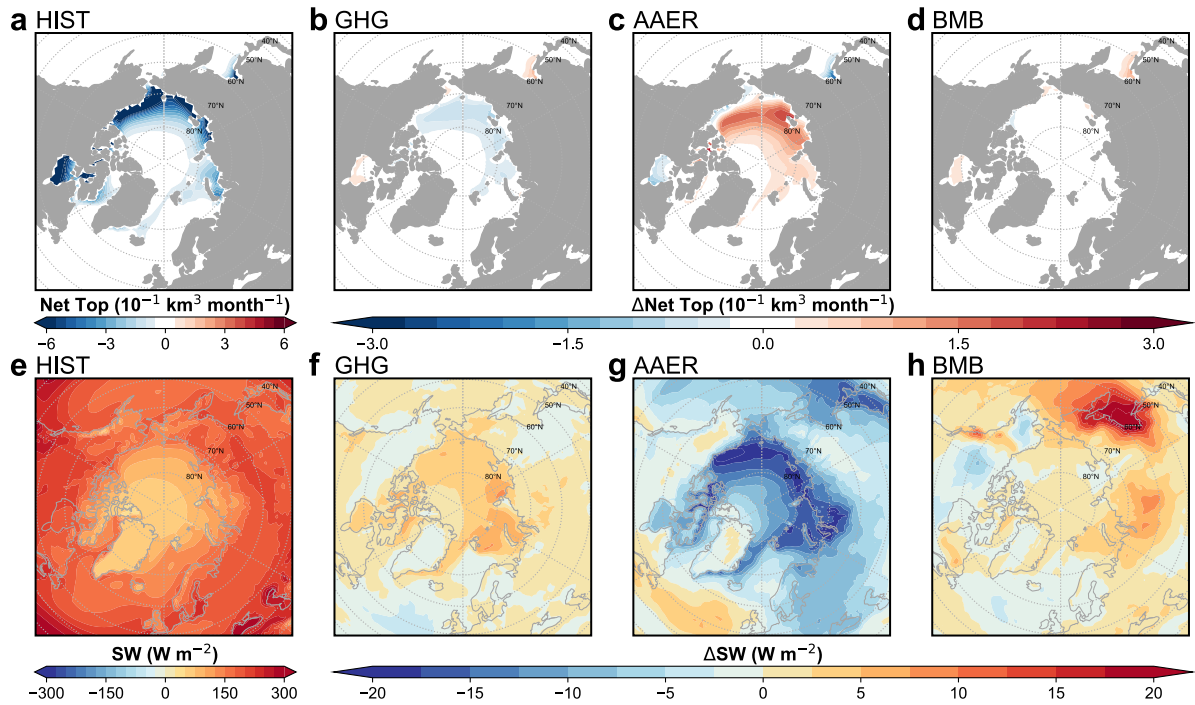


Fig 6: Summer (JJA) Arctic sea ice volume tendencies and shortwave radiation fluxes (1956-1980) under different forcing agents in CESM1. Summer (JJA) ensemble mean of (a-d) net sea ice volume tendencies at the top (frazil + melt, shading in $10^{-1} \text{ km}^3 \text{ month}^{-1}$) and (e-h) surface net shortwave radiation fluxes (positive downward, shading in W m^{-2}) for the period 1956-1980. (a,e) for historical climate forcings (HIST), (b,f) for well-mixed greenhouse gases (GHG), (c,g) for anthropogenic aerosols (AAER), and (d,h) for biomass burning (BMB).

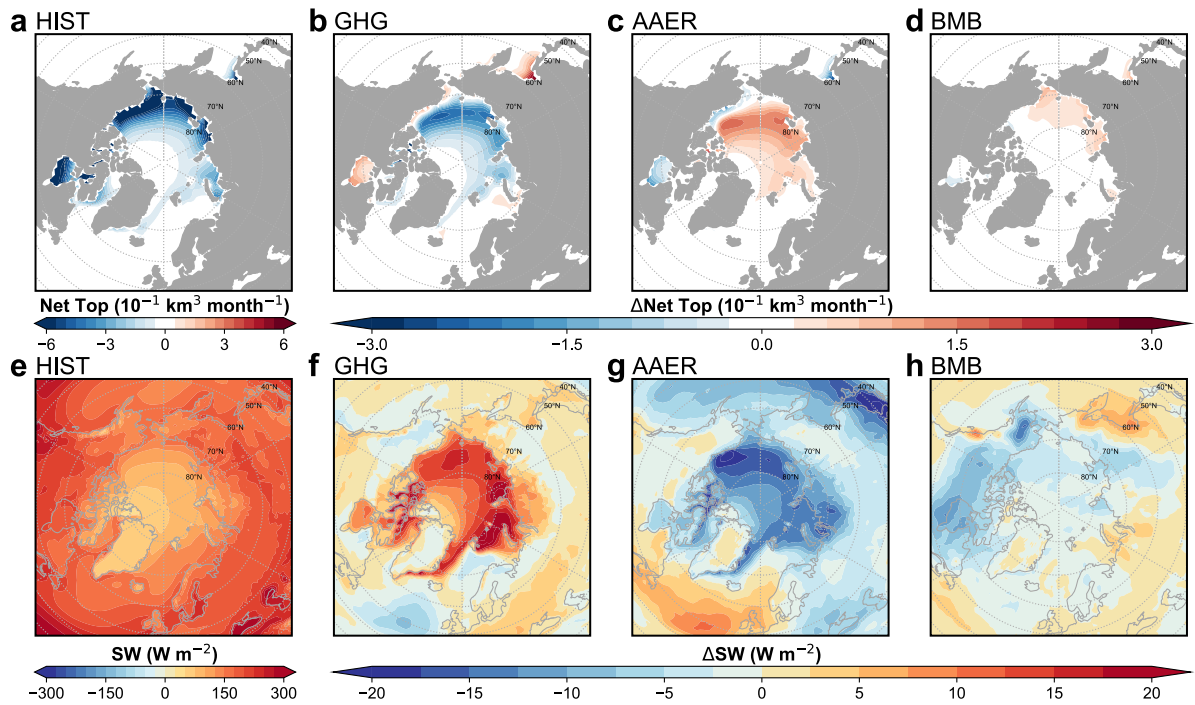


Fig 7: Summer (JJA) Arctic sea ice volume tendencies and shortwave radiation fluxes (1981-2005) under different forcing agents in CESM1. Summer (JJA) ensemble mean of (a-d) net sea ice volume tendencies at the top (frazil + melt, shading in $10^{-1} \text{ km}^3 \text{ month}^{-1}$) and (e-h) surface net shortwave radiation fluxes (positive downward, shading in $W \text{ m}^{-2}$) for the period 1981-2005. (a,e) for historical climate forcings (HIST), (b,f) for well-mixed greenhouse gases (GHG), (c,g) for anthropogenic aerosols (AAER), and (d,h) for biomass burning (BMB).

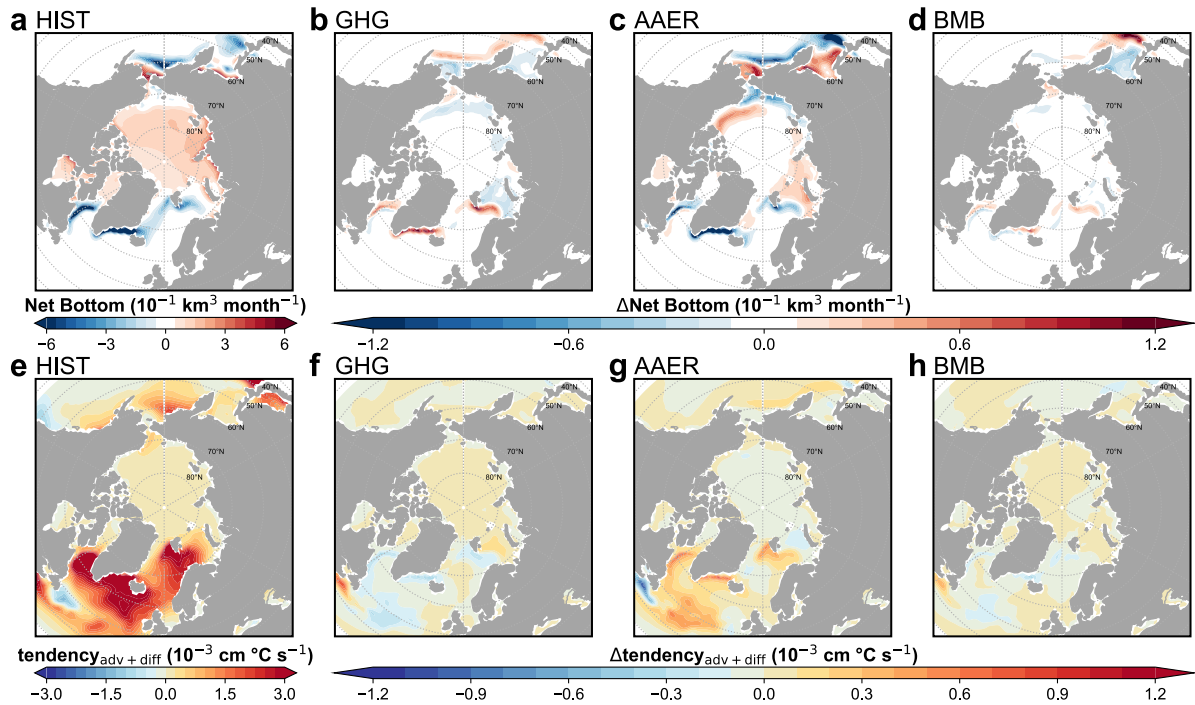


Fig 8: Arctic sea ice volume tendencies and ocean temperature changes (1956-1980) induced by different forcing agents in CESM1. Annual and ensemble mean of (a-d) net sea ice volume tendencies at the bottom (congel + meltb, shading in $10^{-1} \text{ km}^3 \text{ month}^{-1}$) and (e-h) whole-depth ocean temperature tendencies induced by advection and diffusion processes (shading in $10^{-3} \text{ cm } ^\circ\text{C s}^{-1}$) for the period 1956-1980. (a,e) for historical climate forcings (HIST), (b,f) for well-mixed greenhouse gases (GHG), (c,g) for anthropogenic aerosols (AAER), and (d,h) for biomass burning (BMB).

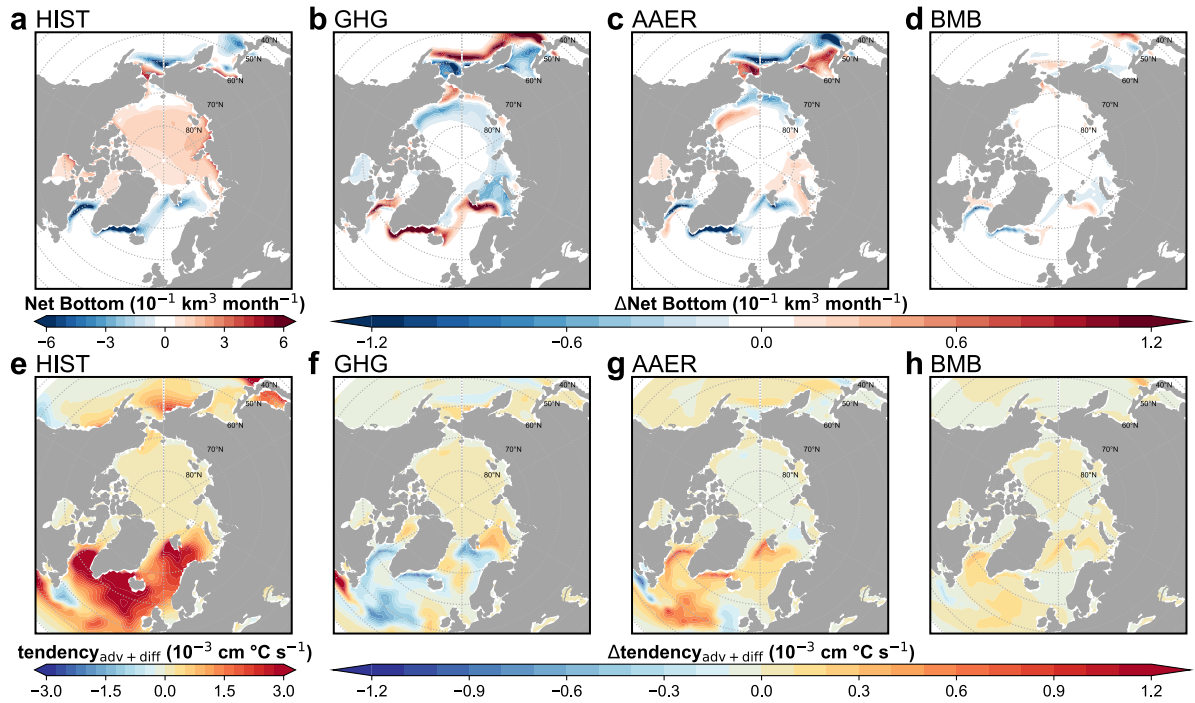


Fig 9: Arctic sea ice volume tendencies and ocean temperature changes (1981-2005) induced by different forcing agents in CESM1. Annual and ensemble mean of (a-d) net sea ice volume tendencies at the bottom (congel + meltb, shading in $10^{-1} \text{ km}^3 \text{ month}^{-1}$) and (e-h) whole-depth ocean temperature tendencies induced by advection and diffusion processes (shading in $10^{-3} \text{ cm } ^\circ\text{C s}^{-1}$) for the period 1981-2005. (a,e) for historical climate forcings (HIST), (b,f) for well-mixed greenhouse gases (GHG), (c,g) for anthropogenic aerosols (AAER), and (d,h) for biomass burning (BMB).